

Single-electron transport in $H_2O@C_{60}$ single-molecule transistors

Bowen Liu(刘博文), Jun Chen(陈俊), Yiping Ouyang(欧阳一平), Minhao Zhang(张敏昊), Yuan-Zhi Tan(谭元植), and Fengqi Song(宋凤麒)

Citation: Chin. Phys. B, 2023, 32 (**6**): 063601. DOI: 10.1088/1674-1056/acc801
Journal homepage: http://cpb.iphy.ac.cn; http://iopscience.iop.org/cpb

What follows is a list of articles you may be interested in

Density functional study on the bimetallic Ti_mZr_n ($n+m \leq 5$) clusters and their interactions with H_2

Ge Zhang(张鸽), Yong Sheng(盛勇)
Chin. Phys. B, 2018, 27 (**9**): 093601. DOI: 10.1088/1674-1056/27/9/093601

Effect of Ni and vacancy concentration on initial formation of Cu precipitate in Fe-Cu-Ni ternary alloys by molecular dynamics simulation

Ke Liu(刘珂), Li-Juan Hu(胡丽娟), Qiao-Feng Zhang(张巧凤), Yao-Ping Xie(谢耀平), Chao Gao(高超), Hai-Ying Dong(董海英), Wan-Yi Liang(梁婉怡)
Chin. Phys. B, 2017, 26 (**8**): 083601. DOI: 10.1088/1674-1056/26/8/083601

Structural optimization of Au-Pd bimetallic nanoparticles with improved particle swarm optimization method

Gui-Fang Shao(邵桂芳), Meng Zhu(朱梦), Ya-Li Shangguan(上官亚力), Wen-Ran Li(李文然), Can Zhang(张灿), Wei-Wei Wang(王玮玮), Ling Li(李玲)
Chin. Phys. B, 2017, 26 (**6**): 063601. DOI: 10.1088/1674-1056/26/6/063601

Structural optimization and segregation behavior of quaternary alloy nanoparticles based on simulated annealing algorithm

Xin-Ze Lu(陆欣泽), Gui-Fang Shao(邵桂芳), Liang-You Xu(许两有), Tun-Dong Liu(刘暾东), Yu-Hua Wen(文玉华)
Chin. Phys. B, 2016, 25 (**5**): 053601. DOI: 10.1088/1674-1056/25/5/053601

A new understanding of inert gas narcosis

Meng Zhang(张萌), Yi Gao(高嶷), Haiping Fang(方海平)
Chin. Phys. B, 2016, 25 (**1**): 013602. DOI: 10.1088/1674-1056/25/1/013602

RAPID COMMUNICATION

Single-electron transport in $H_2O@C_{60}$ single-molecule transistors

Bowen Liu(刘博文)[1,†], Jun Chen(陈俊)[1,†], Yiping Ouyang(欧阳一平)[1], Minhao Zhang(张敏昊)[1,3,‡], Yuan-Zhi Tan(谭元植)[2], and Fengqi Song(宋凤麒)[1,3]

[1] *National Laboratory of Solid State Microstructures, Collaborative Innovation Center of Advanced Microstructures, and School of Physics, Nanjing University, Nanjing* 210093, *China*

[2] *State Key Laboratory of Physical Chemistry of Solid Surfaces, College of Chemistry and Chemical Engineering, Xiamen University, Xiamen* 361005, *China*

[3] *Atom Manufacturing Institute (AMI), Nanjing* 211805, *China*

(Received 17 January 2023; revised manuscript received 21 March 2023; accepted manuscript online 28 March 2023)

Single-molecule transistors (SMTs) based on fullerenes and their derivatives have been recognized as a long-sought platform for studying the single-electron transport properties. $H_2O@C_{60}$ is a combination of fullerene and H_2O, a typical light molecule. Here we use the 'molecular surgery' technique to synthesize the $H_2O@C_{60}$ molecule and then construct the $H_2O@C_{60}$ SMTs, together with the C_{60} SMTs. Evidences for single-electron transport have been obtained in our measurements, including explicit Coulomb blockade and Coulomb oscillations. We then calculate the detailed parameters of the $H_2O@C_{60}$ and C_{60} SMTs using a capacitance model derived from the Coulomb diamond feature, which gives a capacitance ratio of 1:5.05:8.52 for the $H_2O@C_{60}$ SMT and 1:29.5:74.8 for the C_{60} SMT. Moreover, the gate efficiency factor α turns out to be 0.0686 in the $H_2O@C_{60}$ SMT, about ten times larger than that in the C_{60} SMT. We propose that the enhanced gate efficiency in $H_2O@C_{60}$ SMT may be induced by the closer attachment of molecular orbital electron clouds to the gate substrate due to polarization effects of H_2O.

Keywords: single-molecule transistor, fullerenes and their derivatives, light molecule, the polarization effect

PACS: 36.40.–c **DOI:** 10.1088/1674-1056/acc801

1. Introduction

The single-molecule transistor (SMT), which is a three-terminal device that allows us to apply both bias and gate voltages, has proved its potential on exploring the electrical characteristics of single molecules.[1–4] In an SMT, a gate electric field is utilized to control the electrostatic potential and hence the charging state of the single molecule.[5,6] Among the molecules of interest as candidates, fullerenes and their derivatives are highlighted by their unique cage-like structures where multiple atomic or molecular species may be embedded.[7–18]

SMTs based on C_{60} and its derivatives have been shown to exhibit distinctive properties, such as nanomechanical oscillations, superconductivity, quantum phase transitions, and the Kondo effect.[19–22] The combination of C_{60} and H_2O was achieved using the 'molecular surgery' technique.[23–26] H_2O is a typical light molecule with the permanent electric dipole, and its eigenstates are well separated in energy relative to k_BT inside C_{60} (k_B stands for the Boltzmann constant).[27]

Quantum rotations of ortho- and para-water have been extensively studied in $H_2O@C_{60}$ molecules since the subtle interactions between the guest H_2O and the fullerene provide an ideal nanoscale laboratory.[28–34] Furthermore, the ortho–para fluctuations have also been demonstrated in $H_2O@C_{60}$ SMTs.[35] The fluctuation between ortho- and para-water states has been demonstrated on timescales shorter than 1 min.[35] However, in another single-molecule junction study of $H_2O@C_{60}$, it was found that H_2O is electrostatically isolated.[36]

In this work, we fabricated SMTs based on $H_2O@C_{60}$ molecules. $H_2O@C_{60}$ molecules were produced by the 'molecular surgery' method and the devices were made by the feedback-controlled electromigration break junction technique (FCEBJ).[15,37,38] Coulomb blockade phenomena and gate-controlled I_{sd}–V_{sd} curves at 2 K successfully verify the single-electron transport. We applied a capacitance model to quantify the Coulomb diamond feature in SMTs and obtained a larger gate efficiency factor in $H_2O@C_{60}$ SMTs compared to C_{60} SMTs, presumably due to the effect of molecular polarization. Polarization effects may induce a shift of the electron cloud towards the substrate, resulting in a larger effective gate capacitance.

2. Method

The $H_2O@C_{60}$ molecules (Fig. 1(a)) were synthesized according to the optimized procedure reported in previous investigations.[23,26] After the preparation of $H_2O@C_{60}$ powders (Fig. 1(b)), we dissolved them in toluene with the concentration of 0.1 mmol/L and preserved it in the glove box with an Ar atmosphere. The diluted solution exhibits a pink color as shown in Fig. 1(b). In Fig. 2(a) we plot the schematic of the

[†]These authors contributed equally to this work.

[‡]Corresponding author. E-mail: zhangminhao@nju.edu.cn

© 2023 Chinese Physical Society and IOP Publishing Ltd

$H_2O@C_{60}$ SMT: upon the gate oxide, an $H_2O@C_{60}$ molecule is trapped in the gap between the source and drain electrodes, and the silicon gate electrode below the oxide extends to the surface, allowing us to apply a gate voltage. The schematic of the C_{60} SMT is similarly plotted in Fig. S1.

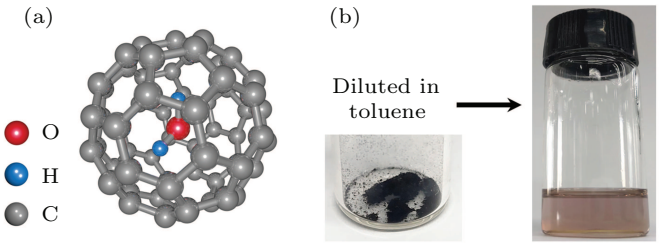


Fig. 1. Synthesis of the $H_2O@C_{60}$ molecules. (a) The simulated structure of a $H_2O@C_{60}$ molecule. The red, blue and gray spheres represent oxygen, hydrogen and carbon atoms, respectively. (b) $H_2O@C_{60}$ molecule powders produced by the 'molecular surgery' technique (left) and 0.1 mmol/L $H_2O@C_{60}$ solution (right) made by dissolving the black powders in toluene.

The essential steps in the construction of the $H_2O@C_{60}$ SMT are as follows. The gate dielectric layer, a $\sim$ 30 nm thick layer of SiO_2, was preferentially formed on Si substrate by the oxidization at 900 °C. The $\sim$ 50 nm wide gold nanowires were fabricated by e-beam lithography and e-beam evaporation on the oxide of the chip (Fig. 2(b)). Before the FCEBJ procedure, we deposited a few drops of $H_2O@C_{60}$ toluene solution onto the surface of the chip in a glove box with an Ar atmosphere. After the evaporation of the solution in the glove box, the chips were wire-bonded to the sample holder and transferred into the measurement system, where the temperature could cool down to 2 K.

Then, we performed the FCEBJ procedure at 2 K to form a nanogap in the $\sim$ 50 nm wide gold nanowires and consequently fabricated the source and drain electrodes (Fig. 2(c)).[15,37,38] In the FCEBJ procedure, the current (conductance) is monitored by the bias voltage which is counter affected by the feedback of current. Once the current drops by 1%, the bias voltage should be reset to 10 mV. The program continues running until the resistance between the source and drain electrodes exceeds 1 MΩ at 20 mV. The diameter of a single $H_2O@C_{60}$ molecule is $\sim$ 1 nm similar to that of C_{60} molecule.[39] The width of gap could be manipulated near 1 nm after the FCEBJ procedure and thus the $H_2O@C_{60}$ molecule can be trapped in the electrode gap successfully. If the $H_2O@C_{60}$ molecule was jammed into the gap, we completed the construction of the SMTs. We also fabricated C_{60} SMTs via the FCEBJ procedure (Fig. S2) by dropping a 0.1 mmol/L solution of C_{60} toluene onto fresh chips.

3. Results

3.1. Single-electron transport in $H_2O@C_{60}$ SMTs

To explore the electron transport properties of the $H_2O@C_{60}$ SMTs, we performed measurements using two Keithley 2450 source meters with voltage applied to the source and gate electrodes, respectively, and the drain electrode was grounded. All the measurements were performed at 2 K to guarantee the stability of the molecular junctions. We show the I_{sd}–V_{sd} curves at the gate voltages of −0.4 V, −0.3 V, −0.2 V, −0.1 V, 0 V in an $H_2O@C_{60}$ SMT (Fig. 2(d)). In the I_{sd}–V_{sd} curves, we can observe a plateau covering the zero-bias point where the current is suppressed, indicating a Coulomb blockade region. The variation of the Coulomb blockade region in Fig. 2(d) implies the gate-controlled chemical potential of the $H_2O@C_{60}$ molecule.

In Fig. 2(e), we calculate the differential conductance dI_{sd}/dV_{sd} as a function of the bias voltage V_{sd} with different gate voltages V_g using the raw data in Fig. 2(d). The differential conductance dI_{sd}/dV_{sd} is calculated numerically with the formula $dI_{sd}/dV_{sd}(V_{sd}) = [I_{sd}(V_{sd}) - I_{sd}(V_{sd} - \Delta V_{sd})]/\Delta V_{sd}$, where ΔV_{sd} is the step size of the bias voltage scanning. In our experiments, ΔV_{sd} is 0.2 mV. The plateau with low differential conductance is plotted against that in the I_{sd}–V_{sd} curve. At the edge of the plateau, several peaks rise, indicating the situation when the electrochemical potential of the molecule matches the Fermi level of the Au electrode. The peaks confirm the Coulomb oscillations. The conductance at the peak is about ten times larger than that at the plateau when V_g equals 0 V. We also observed the clear Coulomb blockage behaviors of the C_{60} SMT (Fig. S3a). At the gate voltage of −3 V, there is a region with relatively low conductance between the two Coulomb oscillation peaks locating at the bias voltages of $\sim$ −0.011 V and $\sim$ 0.024 V (Fig. S3b), which is the Coulomb blockade region. At the gate voltage of −2.25 V, the two peaks merge into one since the situation is close to the resonant tunneling.

Then we map the differential conductance dI_{sd}/dV_{sd} patterns as sweeping the bias voltage V_{sd} and the gate voltage V_g within a certain range in $H_2O@C_{60}$ and C_{60} SMTs, respectively (Figs. 3(a) and 3(b)). Regions with small conductance are colored by blue, while those with large conductance are colored by red. To distinguish the Coulomb blockade regions, the black dashed lines are drawn following the trail of the Coulomb diamond edges. The observation of Coulomb diamonds serves as significant evidence for the existence of Coulomb oscillations, which are characterized by the charging and discharging behavior observed in the Coulomb island. Each time the electrochemical potential and the Fermi levels of the source and drain electrodes are equal, a degeneracy point for resonant tunneling is created where the two black dashed lines cross each other. The high conductance regions above and below the degeneracy point correspond to the case where the molecular potential is locked within a window defined by the Fermi levels of the source and drain electrodes. Otherwise, the molecule acts as a barrier to avoid the passage of electrons. Moreover, we can observe an excited state with the excitation energy of $\sim$ 15 meV indicated by the black arrow,

which may correspond to a vibrational mode induced by the relative motion of H_2O molecule and the C_{60} cage.[35] Due to the large gap between the highest occupied molecular orbital (HOMO) and lowest unoccupied molecular orbital (LUMO) of $H_2O@C_{60}$ and C_{60}, we only access one degeneracy point, which is consistent with the previous studies.[6,21,22,40,41]

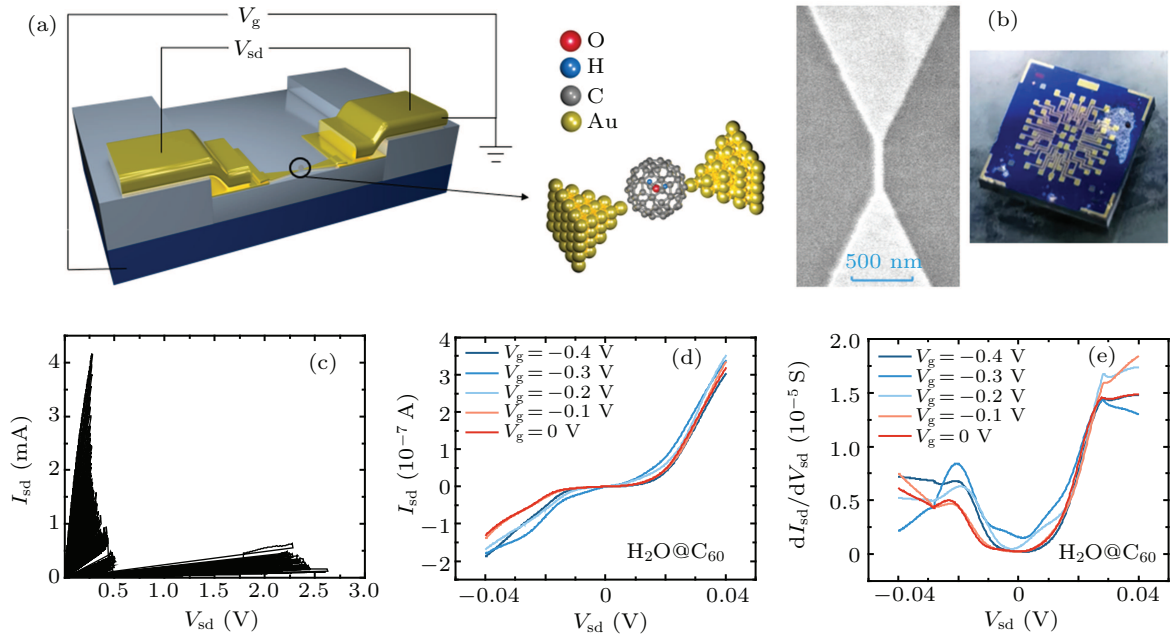


Fig. 2. Coulomb blockade and Coulomb oscillations in an $H_2O@C_{60}$ SMT. (a) The structure of an $H_2O@C_{60}$ SMT (left) and the schematic of the molecule junctions based on it (right) formed by the FCEBJ method. (b) SEM image of the ~ 50 nm wide nanowire before electromigration (left) and a full view of a chip containing 40 junctions. (c) Bias current versus bias voltage during a FCEBJ process. (d) Representative I_{sd}–V_{sd} curves after the electromigration for five different gate voltages in an $H_2O@C_{60}$ SMT. The significant difference between the curves indicates the successful manipulation of the molecular chemical potential by gate voltages. (e) Calculated differential conductance dI_{sd}/dV_{sd} as a function of the bias voltage V_{sd} with various gate voltages V_g using the raw data in (d).

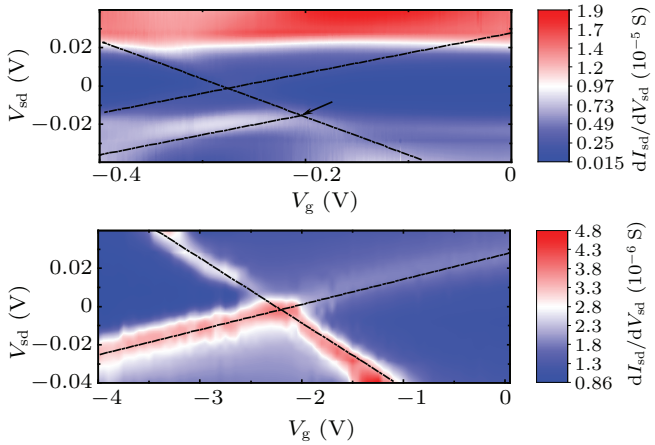


Fig. 3. Two-dimensional plots of the differential conductance dI_{sd}/dV_{sd} versus the bias voltage V_{sd} and the gate voltage V_g in $H_2O@C_{60}$ and C_{60} SMTs. The gate voltage increases from −0.4 V to 0 V in (a), and sweeps from −4 V to 0 V in (b). We can see the distinct Coulomb diamond patterns, indicated by the black dashed lines. The excitation indicated by the black arrow confirms the presence of the $H_2O@C_{60}$ molecule bridging the junction. According to the capacitance model, the capacitance ratio C_g: C_s : C_d is 1:5.05:8.52, and the gate efficiency factor α is 0.0686 in the $H_2O@C_{60}$ SMT. For C_{60} SMT, C_g : C_s: C_d is 1:29.5:74.8, and α is 0.00950.

3.2. Analysis of the large gate efficiency factor

Then, we try to get the detail parameters of $H_2O@C_{60}$ and C_{60} SMTs by applying a capacitance model.[42] In this model, the molecular quantum dot is isolated from the source, drain and gate electrodes by three capacitors, denoted as C_s, C_d and C_g, respectively. If the chemical potential on the molecule equals to that on the source, a line crossing the degeneracy point with the positive slope $\beta = C_g/(C_g + C_d)$ would be generated; the other line, which also goes through the point with a negative slope $-\gamma = -C_g/C_s$, is generated when the chemical potential on the molecule equals that on the drain. Thus, we can compute the capacitance ratio $(C_g : C_s : C_d)$ of the two devices in Fig. 3, that is, 1:5.05:8.52 for the $H_2O@C_{60}$ SMT, and 1:29.5:74.8 for the C_{60} SMT. As seen in other single-molecule junctions reported,[22,38,41] the C_d/C_s ratios are also not equal to 1 in our devices, indicating the asymmetry electron transport of our single-molecule junctions.

Due to the asymmetry, we plot the two-dimensional maps of the the rectification ratios (*RR*s) as a function of V_{sd} and V_g in $H_2O@C_{60}$ (Fig. 4(a)) and C_{60} (Fig. 4(b)) SMTs. The *RR* is defined as $RR(V_{sd}) = |I(V_{sd})/I(-V_{sd})|$. Regions with $RR < 1$ are colored by blue, while regions with $RR > 1$ are colored with red. Both devices show the reversion of rectification when V_g keeps increasing. This distinctive behavior may be related to the tidal diode.[38] We calculate the *RR*s of ~ 10 in our single-molecule junctions.

Additionally, we calculate the gate efficiency factor α, which equals $C_g/(C_g + C_s + C_d)$ and turns out to be 0.0686 ($H_2O@C_{60}$ SMT) and 0.00950 (C_{60} SMT), where $e\alpha V_g$ equals to the shift of the molecule energy level caused by the change

of gate voltage V_g and e is the electron charge. We find that the gate efficiency factor α of $H_2O@C_{60}$ SMT is one order of magnitude higher than that of C_{60} SMT, which indicates the conductance in $H_2O@C_{60}$ SMT is more sensitive to the change of gate voltage. The larger gate efficiency factor α means that the value of C_g is possible enhanced. Because of the value of $\alpha \sim 0.01$–0.001, C_s (C_d) is thus much larger than C_g, and hardly to be changed a lot.

To explain the enhancement in α of the $H_2O@C_{60}$ SMT qualitatively, one possible situation is that the electron cloud distribution of the $H_2O@C_{60}$ molecule is shifted towards the substrate due to the existence of H_2O. Recent research supports this conjecture due to the H_2O polarization.[43] The presence of the water molecule results in a higher electron density at the positions where the hydrogen atoms point to on the carbon cage. Consequently, the electron cloud distribution is shifted towards the gate substrate, and the value of C_g is possible enhanced as seen in Fig. 5(a), leading to an enhanced modulation of the current through the single molecule by the gate voltage. This is also demonstrated in our density functional theory (DFT) results qualitatively. We calculated the electron cloud distribution of HOMO and LUMO in a single $H_2O@C_{60}$ molecule (Fig. 5(b)). As we can see, the H_2O results in a slightly higher electron density at the positions where the hydrogen atoms point to as illustrated by the red arrows. The effect of dipole moment on the gate efficiency factor has also been observed in $Ce@C_{82}$ SMTs.[44] Except the variation of electron cloud distribution induced by the embedded H_2O molecule, other mechanisms might also play a role in the large gate efficiency, such as large dielectric permittivity in $H_2O@C_{60}$.[45]

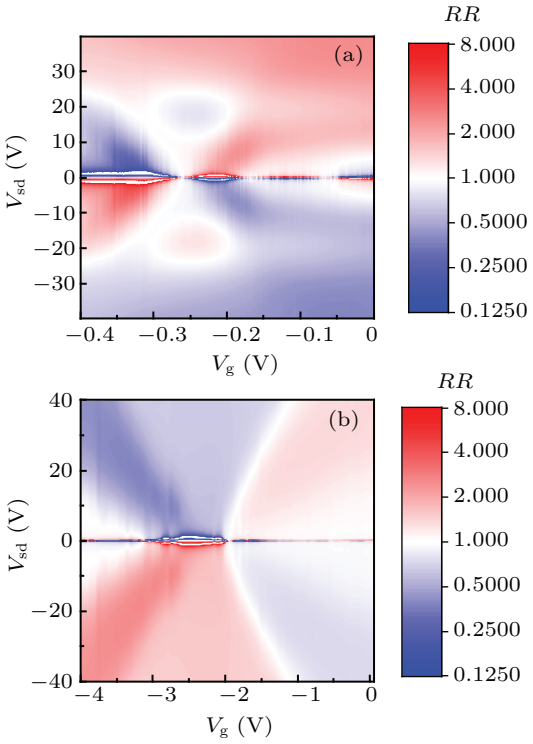


Fig. 4. Two-dimensional plots of the rectification ratios versus the bias voltage V_{sd} and the gate voltage V_g in $H_2O@C_{60}$ ((a)) and C_{60} ((b)) SMTs. The rectification ratio is defined as $RR(V_{sd}) = |I(V_{sd})/I(-V_{sd})|$.

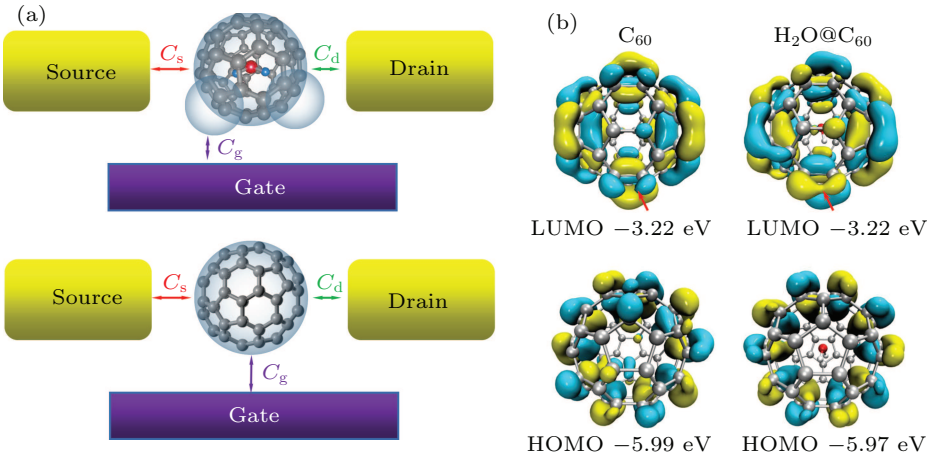


Fig. 5. The possible junction configurations of $H_2O@C_{60}$ and C_{60} SMTs. (a) The electric dipole moment of the water molecule, for some reason, is oriented towards the gate substrate, which results in a higher charge density at the positions where the hydrogen atoms point to on the carbon cage. Consequently, the electron cloud distribution is shifted towards the gate, leading to an enhanced modulation of the current through the single molecule by the gate voltage. (b) The electron clouds of the HOMO and LUMO in C_{60} and $H_2O@C_{60}$ molecules. Compared to C_{60}, the electron density of LUMO in $H_2O@C_{60}$ is increased near the hydrogen atom (indicated by the red arrow).

4. Conclusion

In summary, we fabricated the $H_2O@C_{60}$ SMTs, as well as C_{60} SMTs, to investigate their electron transport properties. The $H_2O@C_{60}$ molecule was synthesized using the 'molecular surgery' technique and the transistors were fabricated using the FCEBJ method. We observed clear Coulomb blockade and Coulomb oscillations in I_{sd}–V_{sd} measurements with varying gate voltages, thus demonstrating single-electron transport in our devices. By introducing a capacitance model, we calculated the gate efficiency factor α from the Coulomb diamond. We obtained a larger α in the $H_2O@C_{60}$ SMT, which may due to the effect of molecular polarization. These findings may

benefit further exploration towards $H_2O@C_{60}$ SMTs and provide helpful information on single-electron transport in alternative devices.

Acknowledgements

We acknowledge the financial support of the National Key R&D Program of China (Grant No. 2022YFA1402), the National Natural Science Foundation of China (Grant Nos. 92161201, T2221003, 12104221, 12104220, 12274208, 12025404, and 12004174), the Natural Science Foundation of Jiangsu Province, China (Grant Nos. BK20200312 and BK20200310), the Fundamental Research Funds for the Central Universities (Grant No. 020414380192).

References

[1] Chen H 2007 *Physics* **36** 910 (in Chinese)
[2] Evers F, Korytár R, Tewari S, *et al*. 2020 *Rev. Mod. Phys.* **92** 035001
[3] Li R H, Liu J Y and Hong W J 2022 *Acta Phys. Sin.* **71** 067303 (in Chinese)
[4] Ouyang Y P, Wang F, Zhang M H, *et al*. 2023 *Adv. in Phys.: X* **8** 2165148
[5] Song H, Kim Y, Jang Y H *et al*. 2009 *Nature* **462** 1039
[6] Guo X and Liang W J 2019 *Chin. Phys. Lett.* **36** 127301
[7] Popov A A, Yang S F, and Dunsch L 2013 *Chem. Rev.* **113** 5989
[8] Lu X, Akasaka T, Slanina Z 2022 *Handbook of fullerene science and technology* (Singapore: Springer Nature Singapore Pte Ltd.) p. 575
[9] Heath J R, O'Brien S C, Zhang Q, *et al*. 1985 *J. Am. Chem. Soc.* **107** 7779
[10] Weiske T, Böhme D K, Hrušák J, *et al.* 1991 *Angew. Chem. Int. Ed. Engl.* **30** 884
[11] Saunders M, Jiménez-Vázquez H A, Cross R J, *et al*. 1993 *Science* **259** 1428
[12] Murphy T A, Pawlik T, Weidinger A, *et al*. 1996 *Phys. Rev. Lett.* **77** 1075
[13] Suetsuna T, Dragoe N, Harneit W, *et al*. 2002 *Chem. Eur. J.* **8** 5079
[14] Komatsu K, Murata M and Murata Y 2005 *Science* **307** 238
[15] Zhang K K, Wang C, Zhang M H, *et al*. 2020 *Nat. Nanotechnol.* **15** 1019
[16] Li J, Hou S J, Yao Y R, *et al*. 2022 *Nat. Mater.* **21** 917
[17] Zhao H Y, Ma H M, Wang J, *et al*. 2016 *Chin. Phys. Lett.* **33** 108105
[18] Gong X F, Wang Y and Ning X J 2008 *Chin. Phys. Lett.* **25** 468
[19] Yu L H and Natelson D 2004 *Nano Lett.* **4** 79
[20] Roch N, Florens S, Bouchiat V, *et al*. 2008 *Nature* **453** 633
[21] Winkelmann C B, Roch N, Wernsdorfer W, *et al*. 2009 *Nat. Phys.* **5** 876
[22] Park H, Park J, Lim A K L, *et al*. 2000 *Nature* **407** 57
[23] Kurotobi K and Murata Y 2011 *Science* **333** 613
[24] Hashikawa Y, Kizaki K, Hirose T, et al. 2020 *RSC Adv.* **10** 40406
[25] Murata Y, Murata M and Komatsu K 2003 *J. Am. Chem. Soc.* **125** 7152
[26] Krachmalnicoff A, Levitt M H and Whitby R J 2014 *Chem. Commun.* **50** 13037
[27] Felker P M, Vlček V, Hietanen I, *et al*. 2017 *Phys. Chem. Chem. Phys.* **19** 31274
[28] Beduz C, Carravetta M, Chen J Y C, *et al*. 2012 *Proc. Natl. Acad. Sci. USA* **109** 12894
[29] Bucher D 2012 *Chem. Phys. Lett.* **534** 38
[30] Li Y J, Chen J Y C, Lei X G, *et al*. 2012 *J. Phys. Chem. Lett.* **3** 1165
[31] Mamone S, Concistrè M, Carignani E, *et al*. 2014 *J. Chem. Phys.* **140** 194306
[32] Goh K S K, Jiménez-Ruiz M, Johnson M R, *et al*. 2014 *Phys. Chem. Chem. Phys.* **16** 21330
[33] Meier B, Mamone S, Concistrè M, *et al*. 2015 *Nat. Commun.* **6** 8112
[34] Meier B, Kouřil K, Bengs C, *et al*. 2018 *Phys. Rev. Lett.* **120** 266001
[35] Du S Q, Hashikawa Y, Ito H, *et al*. 2021 *Nano Lett.* **21** 10346
[36] Kaneko S, Hashikawa Y, Fujii S, *et al*. 2017 *Chem. Phys. Chem.* **18** 1229
[37] Hu K J, Yan W C, Zhang M H, *et al*. 2022 *Nanotechnology* **33** 502001
[38] Zuo Z W, Yan W C, Zhang K K, *et al*. 2022 *AIP Adv.* **12** 095104
[39] Liu S Z, Lu Y J, Kappes M M, *et al*. 1991 *Science* **254** 408
[40] Yoshida K, Hamada I, Sakata S, *et al*. 2013 *Nano Lett.* **13** 481
[41] Pasupathy A N., Park J, Chang C, *et al*. 2005 *Nano Lett.* **5** 203
[42] Tijssen J M and Van der Zant H S J 2008 *Phys. Stat. Sol. (b)* **245** 1455
[43] Zhu G Z, Liu Y, Hashikawa Y, *et al*. 2018 *Chem. Sci.* **9** 5666
[44] Okamura N, Yoshida K, Sakata S, *et al*. 2015 *Appl. Phys. Lett.* **106** 043108
[45] Aoyagi S, Hoshino N, Akutagawa T, *et al*. 2014 *Chem. Commun.* **50** 524